Dilsad Dolunay Eslek Koyuncu*

Mesoporous KIT-6 supported Cr and Co-based catalysts for microwave-assisted non-oxidative ethane dehydrogenation

https://doi.org/10.1515/ijcre-2020-0203
Received October 13, 2020; accepted January 23, 2021;
published online February 8, 2021

Abstract: In the present study, mono and bi-metallic catalysts containing Cr and Co were prepared by impregnating the hydrothermally prepared mesoporous KIT-6 support with 5–10 wt% total metal content. The well-ordered three-dimensional mesoporous structure of the KIT-6 support was confirmed by small angle X-ray diffraction (XRD) patterns. N_2 adsorption-desorption analysis results showed that the mesoporous structure of KIT-6 was preserved after metal loading. Structural bonds of KIT-6 support and prepared catalysts were determined by Fourier-transform infrared (FT-IR) spectroscopy. The pyridine adsorbed diffuse reflectance FT-IR (DRIFT) spectroscopy results revealed the presence of Lewis acid sites on the surface of the catalysts. Activity experiments were carried out in a microwave-heated continuous-flow fixed bed reactor system at temperature range of 350–650 °C and feed ratios of Ethane/Argon: 1/2, 1/1, 2/1 with a gas hourly space velocity (GHSV) of 18,000 ml/h.g_{cat}. The 5Cr@KIT-6 catalyst exhibited high ethane conversion (63.5%) while the highest ethylene/hydrogen ratio (0.98) was obtained with the 2.5Cr2.5Co@KIT-6 catalyst at 450 °C. It was concluded that high temperatures (above 450 °C) facilitate the formation of side reactions and the production of aromatic compounds. The high catalytic activities of mesoporous catalysts were thought to be due to hot spots in the microwave reactor system.

Keywords: Co; Cr; ethane dehydrogenation; KIT-6 support; microwave heated reactor; non-oxidative.

1 Introduction

Hydrogen is considered to be the clean energy carrier that is believed to be able to solve the world energy problem and reduce environmental pollution (Rahmanzadeh and Taghizadeh 2019). Hydrogen production processes include steam reforming, dry reforming, autothermal reforming, partial oxidation reforming, carbon gasification, water gas shift reaction, water electrolysis and hydrocarbon decomposition (Vincent and Bessarabov 2018). The non-oxidative dehydrogenation of ethane (R1) is noteworthy as it produces hydrogen and ethylene as a by-product.

$$C_2H_6 \leftrightarrow C_2H_4 + H_2 \quad \Delta H^0_{298} = 136.0 \ \ kJ/mol \qquad (R1)$$

Ethylene is one of the most important building blocks of the chemical industry. It is used as a feedstock in the production of liquid hydrocarbons (Jan and Resende 2018), polyethylene (Quijada et al., 2001), polyvinyl chloride (Ahn et al. 2018), ethylene glycol (Liu et al. 2018b; Lu et al. 2018), vinyl acetate (Huang et al. 2017), acetaldehyde (Jira 2009) etc. The steam cracking of ethane is the industrial-scale production route for ethylene production (Sun et al. 2011; Wang et al. 2019). However, this reaction is carried out at elevated temperatures (above 1100 K) and ethylene selectivity is not high (Sun et al. 2011). Non-oxidative catalytic ethane dehydrogenation reaction which can be carried out at lower temperatures is seen as more economical and environmental route for ethylene production (Ji et al. 2018). Methane (CH_4) and coke (C) are two important side products of ethane dehydrogenation. Related reactions are as follows:

$$C_2H_6 \rightarrow 3H_2 + 2C \quad \Delta H^0_{298} = 84.7 \ \ kJ/mol \qquad (R2)$$

$$C_2H_6 \rightarrow CH_4 + H_2 + C \quad \Delta H^0_{298} = 9.3 \ \ kJ/mol \qquad (R3)$$

$$C_2H_6 \rightarrow CH_4 + 1/2C_2H_4 \quad \Delta H^0_{298} = 35.6 \ \ kJ/mol \qquad (R4)$$

$$C_2H_4 \rightarrow CH_4 + C \quad \Delta H^0_{298} = -127.1 \ \ kJ/mol \qquad (R5)$$

$$CH_4 \leftrightarrow C + 2H_2 \quad \Delta H^0_{298} = 74.5 \ \ kJ/mol \qquad (R6)$$

Coke deposition on the catalyst surface leads to the catalyst deactivation. While methane can be formed as a result of ethane decomposition (R3 and R4) and ethylene decomposition (R5) reactions, coke can be obtained from ethane decomposition (R2 and R3), ethylene decomposition (R5) and reversible methane decomposition (R6) reactions. Other side products such as acetylene, butene,

***Corresponding author: Dilsad Dolunay Eslek Koyuncu**, Department of Chemical Engineering, Gazi University, 06570, Ankara, Turkey, E-mail: deslek@gazi.edu.tr. https://orcid.org/0000-0001-8092-6740

propylene, benzene and toluene can be formed according to the following reactions:

$$C_2H_4 \rightarrow C_2H_2 + H_2 \quad \Delta H^0_{298} = 175.0 \ \ kJ/mol \qquad (R7)$$

$$2C_2H_4 \rightarrow C_4H_8 \quad \Delta H^0_{298} = -103.4 \ \ kJ/mol \qquad (R8)$$

$$C_4H_8 + C_2H_4 \rightarrow 2C_3H_6 \quad \Delta H^0_{298} = -12.6 \ \ kJ/mol \qquad (R9)$$

$$3C_2H_4 \rightarrow C_6H_6 + 3H_2 \quad \Delta H^0_{298} = -73.9 \ \ kJ/mol \qquad (R10)$$

$$7C_2H_4 \rightarrow 2C_7H_8 \rightarrow 6H_2 \quad \Delta H^0_{298} = -265.9 \ \ kJ/mol \qquad (R11)$$

By using the appropriate catalyst, it is possible to minimize these side reactions and thus increase hydrogen selectivity. Platinum-based catalysts are reported as the most active catalyst for ethane dehydrogenation. However, this noble metal has high cost and when used in its pure form, it suffers from rapid catalyst deactivation. In recent years, researchers have focused on producing hydrogen using catalysts with low cost and high hydrogen selectivity. Transition metal catalysts have attracted attention in this respect. In the literature studies, Mo (Heracleous and Lemonidou 2006; Ji et al. 2018), Ga (Ausavasukhi and Sooknoi 2014; Leth et al. 2008), Cr (Ahn et al. 2018; Tsyganok et al. 2007), Pt (Dangwal et al. 2017; Sun et al. 2011), In (Wegener et al. 2018), Sn (Wu et al. 2014), Fe (Shen et al. 2007) and Ni (Shen et al. 2007) based catalysts were investigated for non-oxidative dehydrogenation of ethane. Cr-containing catalysts were reported as showing high catalytic activity during the dehydrogenation of light alkanes (Bugrova et al. 2019; Rahmani, Haghighi, and Amini 2015). To achieve stable catalytic performance, it was stated that the distribution of Cr species on supports with high surface area is very important. In addition, the incorporation of the second metal into the catalyst may lead to the decrease in the reduction temperature, decrease in crystallite size of active metal and increase in catalytic activity (Megia et al. 2019).

In the hydrogen production reactions, silica-based support materials are preferred because of their superior properties such as high surface area, good metal-support interaction, easy production steps, high thermal and mechanical strength (Ruelas-Leyva et al. 2018; Zhang et al. 2013). KIT-6 material, which is a cubic Ia3d form of mesoporous silica, has been firstly synthesized by Korea Advanced Institute of Science and Technology (KAIST). It has interpenetrating bi-continuous pore system, and tunable pore size of this material makes it more advantageous than other silica materials (Li et al. 2017; Wang et al. 2014). By changing the synthesis conditions such as hydrothermal treatment temperature, surfactant type and surfactant concentration, the pore size of KIT-6 material can be tuned from 4 to 12 nm (Kleitz, Choi, and Ryoo 2003). The most important reason of using this material as a support material is the unique 3D interpenetrating pore structure which allows direct and open access of guest molecules without pore blocking (Chirra et al. 2019; Li et al. 2017; Taghizadeh, Akhoundzadeh, and Rezayan 2018). KIT-6 materials can be prepared by typical hydrothermal synthesis procedure given in Figure 1. Synthesis is performed in acidic medium of HCl. Triblock co-polymer P123 (PEO-PPO-PEO) and tetraethyl orthosilicate (TEOS) are used as surfactant and silica source, respectively. The main difference of the synthesis of KIT-6 material from SBA-15 synthesis is using 1-butanol as co-solvent and co-surfactant (Fernandes et al. 2018). It has been reported that 1-butanol provides phase transformation and low amounts of this (1-butanol/P123 < 0.9 by weight) cause the formation of 2D hexagonal mesophase (Kleitz, Choi, and Ryoo 2003).

Unlike conventional heating, microwave heating includes an energy conversion from electromagnetic energy to thermal energy. In the microwave systems, energy is transferred within the material through the molecular interaction with the electromagnetic field (Sun, Wang, and Yue 2016). It was reported that in heterogeneous catalytic systems, microwave heating provides energy efficiency by reducing bulk catalyst temperatures and obtaining higher selectivity due to repressing side reactions of undesired products. Activity increase is attributed to the formation of localized hot spots in the catalyst bed (Robinson et al. 2020). In addition, microwave reactors have the advantages of thermal control ability thanks to their high heating rate and instant on-off feature. The selective heating of material, rapid heating, contactless heating and portability are the other important advantages of microwave systems (Sun, Wang, and Yue 2016). In the literature, microwave heating systems have been used in different reactions, such as dry reforming of methane (Tan et al. 2019), gasification of biomass (Ke et al. 2019), NO decomposition (Xu et al. 2016), NH_3 synthesis (Bai

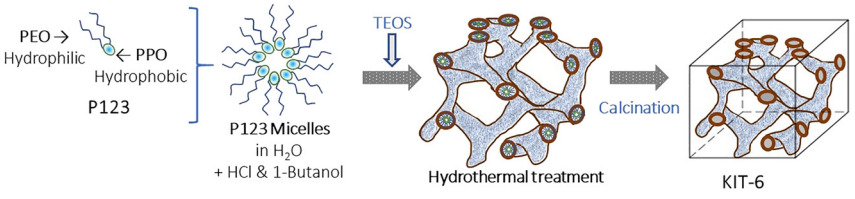

Figure 1: Typical synthesis mechanism of KIT-6 materials.

et al. 2018; Wildfire et al. 2018) and NH_3 decomposition (Varisli, Korkusuz, and Dogu 2017). Studies on non-oxidative ethane dehydrogenation in the microwave heating reactor system are limited (Kim et al. 2001; Ng et al. 2013; Robinson et al. 2020). There is a new study in the literature related with using microwave heating in the catalytic dehydrogenation of ethane (Robinson et al. 2020). They compared the catalytic results of conventional heating and microwave heating systems and concluded that while microwave heating enhances the selectivity to ethylene and hydrogen, conventional heating system leads to the formation of aromatics. Moreover, to achieve the same ethane conversion in microwave heating at 375 °C, the temperature had to be increased to 660 °C in conventional system (Robinson et al. 2020). This result is an indication of energy saving advantage of microwave heating which is very important especially for endothermic catalytic reaction systems. In the study of Ng et al. (Ng et al. 2013), it was concluded that minimum 30% of energy saving was possible in the microwave heating systems. Kim et al. (2001) investigated non-oxidative ethane dehydrogenation over $Pt/\gamma\text{-}Al_2O_3$ and $Pd/\gamma\text{-}Al_2O_3$ catalysts. They reported that higher ethylene yield and selectivity can be obtained at lower temperatures compared to the conventional systems.

In this study, mesoporous KIT-6 supported Cr and Co-containing mono-metallic and bi-metallic catalysts were prepared for hydrogen production via ethane dehydrogenation. It has been reported in the literature the Cr-based catalysts are preferred over Pt-based catalysts for the dehydrogenation of light alkanes due to their lower cost (Saito and Sekine 2020). The C-H cracking ability of Co-based catalysts is also remarkable (Megia et al. 2019). Various characterization techniques were used to determine the effect of metal incorporation on the structural properties of KIT-6 support. The catalytic activity tests were carried out in a microwave heated reactor system in different feed compositions and at different reaction temperatures.

2 Experimental

2.1 Synthesis of mesoporous KIT-6 material

Mesoporous KIT-6 materials were prepared by hydrothermal synthesis procedure as reported in the literature (Ayad et al. 2016). Typically, until reaching complete dissolution 6 g of surfactant, Triblock copolymer Pluronic P123 (poly(ethylene oxide)-poly(propylene oxide)-poly(ethylene oxide), Sigma-Aldrich, molecular weight ≈ 5800), 220 ml of deionized water and 12 g of concentrated HCl (Sigma-Aldrich, 37%) were stirred at 35 °C. The concentrated HCl was used as co-solvent in the synthesis of KIT-6 material. Then, 6 g of co-surfactant 1-Butanol (Alfa Aesar, 99%) was added to this mixture. After 1 h mixing at the same temperature, 12.4 g of Tetraethyl orthosilicate, TEOS (Sigma-Aldrich, 98%) was added as silica source. Mixing was carried out for 24 h at the same temperature. The resulting mixture was transferred to a Teflon lined autoclave, and hydrothermal treatment was performed under static conditions at 120 °C for 24 h. The solid product was recovered by vacuum filtration and washed with deionized water several times until the pH of the filtrate remained constant. The solids were oven dried at 90 °C and calcined at 750 °C for 6 h with a heating rate of 10 °C/min in air flow.

2.2 Synthesis of Cr–Co-containing KIT-6 supported catalysts

Mono-metallic and bi-metallic Cr–Co-containing KIT-6 supported catalysts were prepared by wet impregnation method in total metal amounts of 5 wt% and at different Cr/Co ratios (Cr/Co ratio by mass 1/1, 1/0, 0/1). Chromium(III) nitrate nonahydrate ($Cr(NO_3)_3.9H_2O$, Sigma-Aldrich, 99%) and cobalt(II) nitrate hexahydrate ($Co(NO_3)_2.6H_2O$, Sigma-Aldrich, 99%) were used as Cr and Co precursors, respectively. In this synthesis procedure, KIT-6 support suspension was prepared using deionized water at 40 °C. Desired amounts of metal salts were dissolved in deionized water, and this solution was added dropwise to the support suspension. Dehydration was carried out while stirring at the same temperature. After impregnation, solids were calcined in dry air at 750 °C for 6 h and reduced with a flow of H_2 at 750 °C for 1 h to obtain final product. The catalysts prepared via this procedure were named as xM@KIT-6, where "x" stands for the weight percent of "M" metal (M = Cr, Co).

2.3 Characterization studies

Crystalline phases of the KIT-6 and KIT-6 supported catalysts were determined by the low-angle and wide-angle powder X-ray diffraction (XRD) analyses, using a Rigaku Ultima-IV diffractometer with Cu Kα radiation (λ = 0.15406 nm, 40 kV and 30 mA) at a scanning rate of 0.2° min^{-1} and 2° min^{-1}, respectively. The N_2 adsorption/desorption isotherms were obtained with Quantachrome Autosorb-1C model equipment, at 77 K. Before the experiments, samples were vacuum dried at 250 °C for 3 h. The specific surface areas of KIT-6 samples were calculated using the desorption points within the N_2 relative pressure range of 0.05–0.30 using Brunauer-Emmett-Teller (BET) method. The pore size distributions of the samples were obtained from the analysis of the desorption values by using the Barrett-Joyner-Halenda (BJH) method. The surface morphologies and the chemical composition of the samples were determined by SEM and EDS analysis using QUANTA 400F Field Emission Scanning Electron Microscopy (FE-SEM) equipment at 30 kV. The structural bonds present in the structure were investigated by Fourier-transform infrared spectroscopy (FT-IR) in the medium infrared region of 4000–400 cm^{-1} with 4 cm^{-1} resolutions in a Jasco 4700 ATR/FT-IR spectrophotometer. The surface acidities of the samples were achieved by diffuse reflectance FT-IR (DRIFT) analysis of pyridine adsorbed samples, using the Jasco 4700 FTIR instrument in the medium infrared region of 1690–1390 cm^{-1}. Pyridine was adsorbed on samples for 2 h at 40 °C prior to DRIFT analysis. In the determination of Lewis and Brønsted acid sites, differences of the DRIFT spectra of pyridine adsorbed and non-adsorbed samples were used.

2.4 Catalytic activity experiments

The synthesized catalysts were tested for non-oxidative dehydrogenation of ethane under microwave-assisted heating in a continuous-flow fixed bed reactor system. The system consists of three parts; feed

gas mixture preparation section, microwave reactor section and product gas analysis section. Two mass flow controllers were employed to feed the reactive gas mixture in a desired ratio. Microwave-heated reactor (SAIREM) consists of three main sections: generator, magnetron and applicator where quartz glass reactor is placed. The power of the microwave is adjusted from the generator that can provide maximum 2 kW of energy. The bulk temperature measurement of the catalyst bed was done with the aid of the infrared pyrometer (Raytek M13) directly from the cavity facing the catalyst bed at a distance of 2 cm. In the experiments, carbon nanofiber material with high dielectric coefficient was used as a microwave receptor. Firstly, 0.05 g of catalyst powder and the same amount of carbon nanofiber were mixed and put into the filtered glass quartz reactor. The reactor was placed in the applicator section of the microwave reactor, which would provide the reaction temperature. Microwave adjusters located above and below the applicator allow the microwave energy to focus directly on the catalyst bed and reach the desired temperature. The gas mixture of the desired composition was prepared on the by-pass line using high purity ethane (Air Products, 99.5%) and argon, and then sent to the system. The gas phase products were analyzed in every 20 min by an online gas chromatograph (GC, Agilent Model 6890N), fitted with a thermal conductivity detector (TCD) and using Ar as a carrier gas. Activity experiments were carried out in the 300–650 °C temperature range with feed ratios of Ethane/Ar: 1/2, 1/1, 2/1 with a GHSV of 18,000 ml/h.g_{cat}.

The activities of the catalysts were determined by calculating the ethane conversion Eq. (1), product (H_2, C_2H_4, CH_4, C_2H_2) selectivity Eq. (2) and product yield Eq. (3) from the following equations:

$$\text{Ethane conversion}\,(\%) = \frac{C_2H_{6in} - C_2H_{6out}}{C_2H_{6in}} \times 100 \quad (1)$$

$$\text{Selectivity of Product } i = \frac{\text{Moles of product } i}{C_2H_{6in} - C_2H_{6out}} \quad (2)$$

$$\text{Yield of product } i = \frac{\text{Moles of product } i}{C_2H_{6in}} \quad (3)$$

3 Results and discussion

3.1 Characterization results

The small angle XRD patterns of the KIT-6 material and KIT-6 supported catalysts are shown in Figure 2. KIT-6 support exhibited three main XRD peaks at 2θ = 1.02°, 1.22° and 1.9°, corresponding to (211), (220) and (332) Miller indices, and the low intensity peaks between 1.5 and 1.8. These are the characteristics of KIT-6 structure which is a well-ordered three-dimensional mesoporous structure with spatial group Ia3d organized in body-centered cubic array (Karthikeyan et al. 2018). The ordered body centered cubic structure was preserved even after 5 wt% metal loading, and the intensity of the diffraction peaks decreased as compared with KIT-6 support. The lowest peak intensities were obtained with 5Co@KIT-6 and 2.5Cr2.5Co@KIT-6 catalysts. This may be attributed to the deterioration of regular crystal structure of KIT-6.

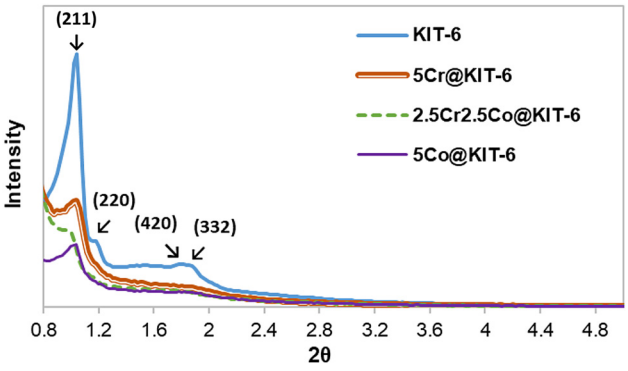

Figure 2: Small angle XRD patterns of KIT-6 support and reduced catalysts.

The wide-angle XRD patterns of KIT-6 supported catalysts are given in Figure 3. All samples have a broad diffraction peak in the range of 2θ = 15°–30°, which is the characteristic of amorphous silica materials (Li et al. 2017). In the XRD patterns of reduced 5Co@KIT-6 catalyst, a relatively broad peak was observed at 2θ = 44.3° which is corresponding to metallic Co species (Alalwan, Cwiertny, and Grassian 2017). The peaks at about 2θ values of 24.62°, 33.72°, 36.32°, 41.42°, 50.30°, 54.98°, 63.56° and 65.12° observed in the XRD patterns of 5Cr@KIT-6 was related with the presence of Cr_2O_3-Eskolaite (File No 6-0504) (Smith and Berry 1974) in the structure. The XRD results of Cr-containing catalysts were found to be consistent with those reported in the literature (Anandhi, Rayer, and Chithambarathanu 2017). A broad peak with a low intensity at 2θ = 36.07° corresponding to Cr_2O_3 structure was observed in the bi-metallic 2.5Cr2.5Co@KIT-6 catalyst, and no peak was observed that is related with Co species. Broader or no diffraction peak in the XRD patterns can be attributed to the small crystallite size of metal particles on the support surface (Zhao et al. 2005). Crystallite sizes of metal particles

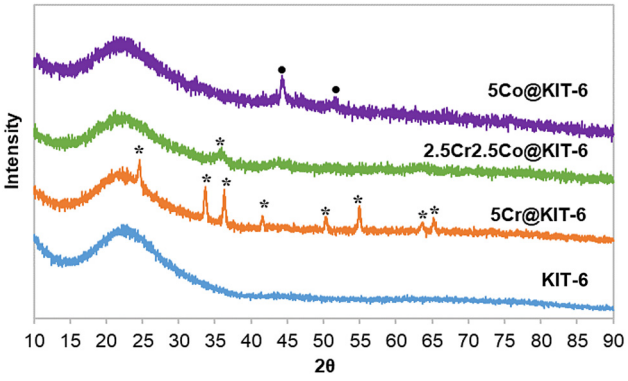

Figure 3: Wide angle XRD patterns of KIT-6 support and reduced catalysts (•Co, ⋆ Cr_2O_3-Eskolaite).

in the catalysts were calculated by Scherrer Equation. The smallest crystallite size of Cr_2O_3 particles on KIT-6 support in 2.5Cr2.5Co@KIT-6 catalyst was also confirmed by the results of Scherrer Equation given in Table 1.

The N_2 adsorption–desorption isotherms of the KIT-6 support and reduced metal catalysts were classified as Type IV (Figure 4). The characteristic behavior of Type IV isotherms can be explained as a sharp capillary condensation step at high relative pressures (nearly at P/P^0 = 0.6–0.8) and a final saturation plateau (Fernandes et al. 2018). Capillary condensation in mesopores larger than 4 nm leads to the formation of hysteresis between adsorption and desorption curves. It is reported that there is a correlation between the shape of the hysteresis loop and the pore properties of the material (Cychosz and Thommes 2018). All catalysts exhibited hysteresis loop in similar relative pressure range starting from P/P^0 = 0.65. The presence of Type IV isotherms in all catalysts means that the mesopore structure is preserved. The narrow hysteresis loop in the N_2 adsorption–desorption isotherm is the indication of the pore system with high uniformity (Fernandes et al. 2018). The narrow hysteresis loop of the KIT-6 support was associated with the highly uniform mesopore structure of this material. It was observed that the N_2 adsorption–desorption isotherms slightly expanded after metal loading. This expected observation can be attributed to the change in pore structure due to the metal loading. In addition, after metal loading the adsorbed volume value decreased because of the partial pore blockage (Chen et al. 2018). XRD and N_2 adsorption–desorption results of the samples were summarized in Table 1. The pore volume and pore diameter of the KIT-6 support determined by BJH method were 1.50 cm^3/g and 7.5 nm, respectively. BET surface area of the support was found to be 726 m^2/g. Total metal contents of the catalysts were determined by EDS analysis. Consistent results were obtained in terms of total metal content in the synthesis solution. Similar results were observed in the literature (Chen et al. 2018; Kishor and Ghoshal 2017; Son, Choi, and Ahn 2008; Xu, Wang, and Guan 2014). Kishor and Ghoshal (2017) found the pore volume, pore diameter and wall thickness of the KIT-6 sample prepared at 120 °C as 1.51 cm^3/g, 8.0 nm and 3.06 nm, respectively. The change in the pore structure after metal loading was also supported by the wall thickness values of KIT-6 support and catalysts. It is seen that the pore volume, pore diameter and BET surface area values of the support decreased slightly after metal loading. Thus, the wall thickness of the support material increased. This result is more evident in the 2.5Cr2.5Co@KIT-6 catalyst. It is seen that this catalyst exhibited the lowest surface area as 531 m^2/g. In the study of Liu et al. (2018a), they prepared 10 wt% Co-containing KIT-6 catalysts at different reduction temperatures. They concluded that the surface area and pore volume were decreased with the increase in the reduction temperature due to the pore blocking at high metal loading. The surface area of the Co-containing KIT-6 catalyst reduced at 550 °C was found as 376 m^2/g (Liu et al. 2018a).

Figure 5 shows the pore size distributions of KIT-6 support and metal-containing catalysts. All samples exhibited narrow and monodisperse pore size distribution in the mesopore range (6–10 nm) according to the IUPAC classification (Thommes et al. 2015). The narrow pore size distribution is associated with the homogeneity of mesoporous structure (Xia et al. 2018). This is another indicative of the preservation of the mesopore structure after metal loading. The preservation of mesopore structure in all catalysts can be attributed to the well-developed mesopore structure of KIT-6 support (Liu et al. 2018a).

Structural bonds of KIT-6 support and prepared catalysts were determined by ATR/FT-IR spectra given in Figure 6. In the ATR/FT-IR spectra of all samples, bands observed around 1054, 810 and 445 cm^{-1} were related with the structural siloxane (Si–O–Si) framework present in the KIT-6 structure. The band at 1054 cm^{-1} and identified shoulder at about 1220 cm^{-1} were the typical bands referring to asymmetric stretching of the Si–O–Si bond (Merkache et al. 2015). Bands at 800 and 445 cm^{-1} were attributed to symmetrical stretching and bending vibrations of the Si–O–Si bond, respectively (Kishor and Ghoshal 2017; Xu et al. 2019). The FT-IR studies of

Table 1: XRD and BET results of KIT-6 support and reduced catalysts.

Sample	d_{211}[a] nm	a_0[b] nm	Wall thickness[c] t, nm	Pore diameter[d] d_p, nm	Pore volume[d] V_p, cm^3/g	Surface area[d] m^2/g	Crystallite size[e] nm	Total metal content[f] wt%
KIT-6	8.49	20.8	2.9	7.5	1.50	726	–	–
5Cr@KIT-6	8.49	20.8	3.6	6.8	0.97	553	23.6	4.8
2.5Cr2.5Co@KIT-6	9.01	22.1	4.4	6.6	0.86	531	5.3	5.3
5Co@KIT-6	8.49	20.8	3.5	6.9	0.99	565	14.6	4.7

[a]Interplanar spacing calculated from Bragg's Law. [b]Cubic parameter, $a_0 = d_{211} * \sqrt{h^2 + l^2 + k^2}$. [c]$t = a_0/2\text{-}d_p$. [d]Obtained from BJH desorption data. [e]Determined by Scherrer Equation. [f]From EDS analysis.

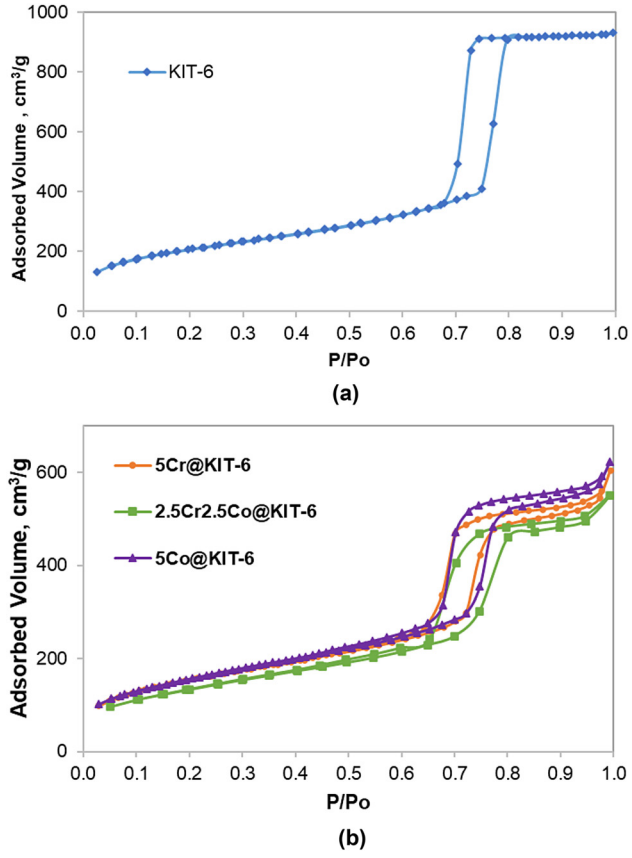

Figure 4: N_2 adsorption–desorption isotherms of (a) KIT-6 support and (b) reduced catalysts.

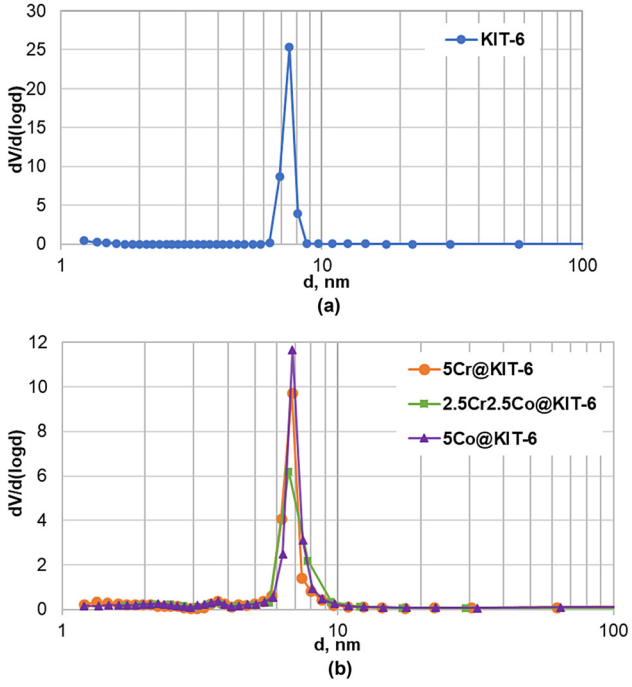

Figure 5: Pore size distributions of (a) KIT-6 support and (b) reduced catalysts.

metal loaded KIT-6 samples confirm that there was no change in functional group after metal impregnation on KIT-6 support. Additionally, in the ATR/FT-IR spectra of 5Cr@KIT-6 sample, small vibration bands at 558 cm^{-1}, 623 cm^{-1} and the identified shoulder at 725 cm^{-1} were related with the Cr–O vibration in crystalline framework of Cr_2O_3 (Dragoi et al. 2013). These results supported the presence of Cr_2O_3 crystal structure as mentioned in XRD results. No peaks were observed that could indicate Co–O bonding in Co-containing catalysts (Gopinatha and Nagarajanb 2015; Qiu et al. 2020). Small vibrations between 1900 and 2400 cm^{-1} are the characteristics of ATR measurements.

The acid sites of the prepared catalysts were determined by diffuse reflectance FT-IR spectroscopy (DRIFTS) using pyridine as probe molecule in the region of 1700–1400 cm^{-1}. In this method, the bands at 1640 cm^{-1} and between 1540 and 1548 cm^{-1} are related with the pyridine adsorbed on Brønsted (B) acid sites, and the band at 1450 cm^{-1} is assigned to adsorption of pyridine on Lewis (L) acid sites. The band appeared between 1490 and 1500 cm^{-1} corresponds to the combination of both B and L acid sites (Moslemi et al. 2019). Additionally, the bands at 1610 and 1577 cm^{-1} are related with the strong and weak Lewis acid sites, respectively (Arbag 2018). It was reported that the peak at about 1595 cm^{-1} was not associated with any acid sites, and this band was assigned to hydrogen-bound pyridine (Taifan, Yan, and Baltrusaitis 2017). Figure 7 shows the DRIFTS result of pyridine adsorbed catalysts. It is seen that the peaks in all samples correspond to Lewis acid sites and Co incorporation to the KIT-6 structure increases the Lewis acid strength (Xu et al. 2014). 5Co@KIT-6 catalyst showed the highest Lewis acid bands among the studied catalyst and no Brønsted acid sites were detected in all samples. The absence of Brønsted acid sites was associated with the basic nature of the catalysts (Taifan, Yan, and Baltrusaitis 2017). It has been reported that surface basicity can contribute to the prevention of coke formation in dehydrogenation (Saito and Sekine 2020).

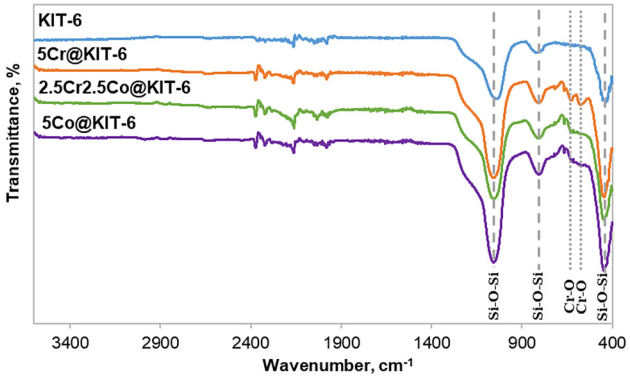

Figure 6: ATR/FT-IR spectra of KIT-6 support and reduced catalysts.

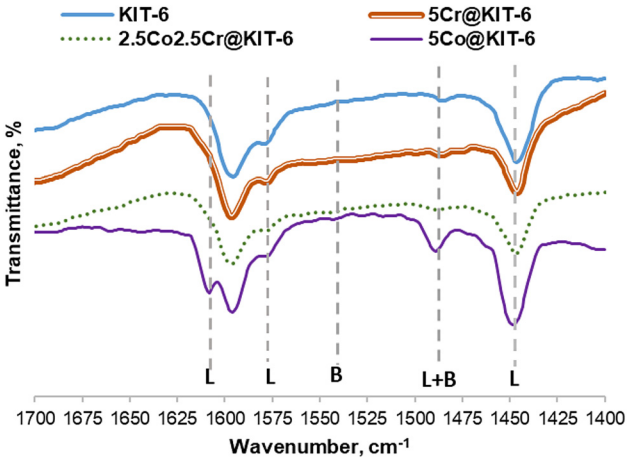

Figure 7: DRIFT result of pyridine adsorbed reduced catalysts.

Heterogeneous particle size distributions of the catalysts were observed in the SEM images of the catalysts (Figure 8).

3.2 Catalytic activity results

In the present study, carbon nanofiber material with high dielectric coefficient was used as a microwave receptor. In each experiment, catalyst powder was physically mixed with the same amount of carbon nanofiber. In the previous study, ethane dehydrogenation over carbon nanofiber was conducted in a microwave heated and conventional heated reactor systems at 450 °C. Carbon nanofiber sample exhibited about 36% ethane conversion in microwave heated reactor system, whereas this sample did not show any catalytic activity in the conventional heated reactor system (Eslek Koyuncu 2020). In order to understand the effect of metal incorporation, Cr and Co-based catalysts were investigated in this study. Microwave-assisted ethane dehydrogenation tests were carried out with KIT-6 supported Cr and Co-containing mono-metallic and bi-metallic catalysts in the temperature range between 350 and 650 °C with feed ratios of Ethane/Argon: 1/2, 1/1, 2/1. Experimental data were collected during 180 min. In the first step of the study, the effect of temperature on the catalytic activity was investigated using 5Cr@KIT-6 catalyst at temperatures ranging between 350 and 650 °C with a feed ratio of Et/Ar:1/2. Figure 9 shows the ethane conversion and selectivity values at different temperatures. It is seen that the ethane conversion increases with the increasing temperature due to the endothermic nature of the ethane decomposition reaction. Catalytic activity results obtained at different temperatures are summarized in Table 2.

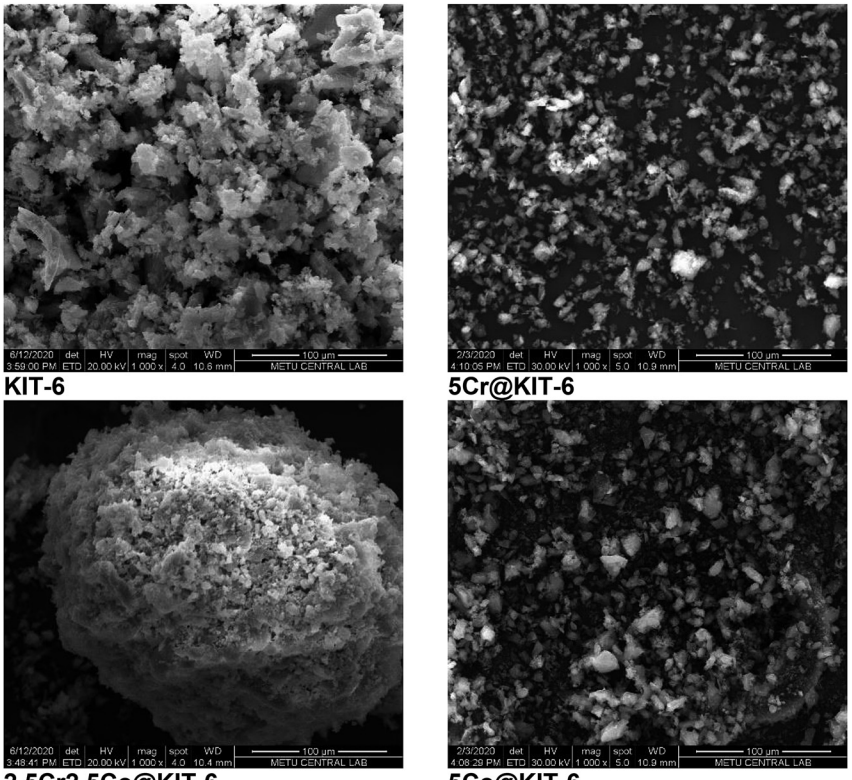

Figure 8: SEM images of KIT-6 support and reduced catalysts.

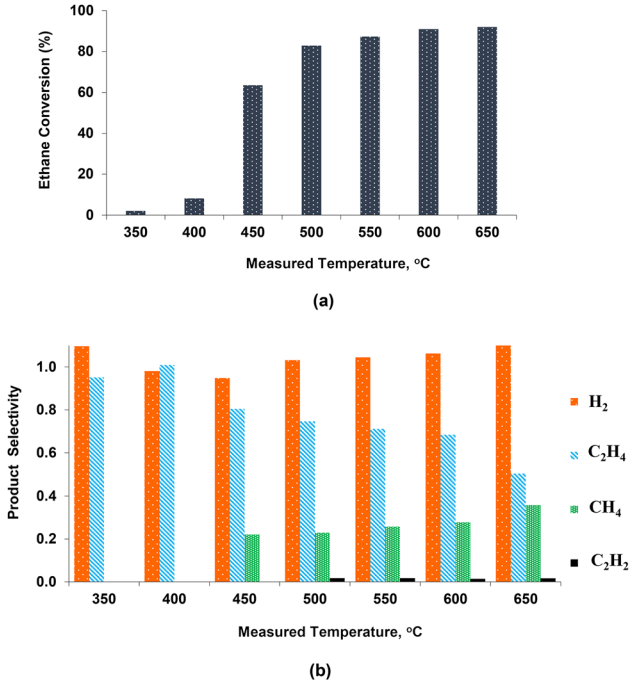

Figure 9: (a) Ethane conversion and (b) product selectivity of 5Cr@KIT-6 catalyst at different temperatures (GHSV: 18,000 ml/h.g_{cat}, Et/Ar: 1/2).

At 400 °C, the ratio of C_2H_4 to H_2 is nearly "1", which is a measure of the absence of side reactions. However, the ethane conversion was about 10% at this temperature. When the temperature increased ($T \geq 450$ °C), side reactions began to occur, and the difference between hydrogen selectivity and ethylene selectivity became higher. The increase in the H_2 yield and the formation of CH_4 and C_2H_2 in the product stream could be attributed to the occurrence of endothermic ethane decomposition (R2: $C_2H_6 \rightarrow 3H_2 + 2C$ R3: $C_2H_6 \rightarrow CH_4 + H_2 + C$ and R4: $C_2H_6 \rightarrow CH_4 + 1/2C_2H_4$) and ethylene decomposition (R5: $C_2H_4 \rightarrow CH_4 + C$ and R7: $C_2H_4 \rightarrow C_2H_2 + H_2$) reactions. After 600 °C, yellowish solid substance which is the indication of aromatic compounds was observed at the outlet end of the quartz reactor. Xiang et al. reported that the aromatization of ethane reached high conversions after 600 °C temperatures (Xiang et al. 2018). It was reported that the composition of the aromatics depends on the reaction temperature. Xylene can be formed at lower temperatures, and as the temperature increases, toluene and benzene are formed respectively (Saito and Sekine 2020). It was concluded that high temperatures favored the occurrence of side reactions and the production of aromatic compounds. As a result, 450 °C temperature was accepted as the suitable temperature to achieve high ethane conversion and H_2–C_2H_4 selectivity.

Non-oxidative ethane dehydrogenation reaction is an endothermic equilibrium reaction. Thermodynamically, high temperatures (above 750 °C) are needed at atmospheric pressures to achieve a high conversion as 60% with conventional heating system. High temperature application is not suitable both in terms of system controllability and energy efficiency. In this study, high-tech microwave-heating system was used to heat the catalyst bed, and a pyrometer was used to measure the bulk temperature. It was reported that in heterogeneous catalytic systems, microwave heating provides energy efficiency by reducing bulk catalyst temperatures and obtaining higher selectivity due to repressing side reactions of undesired products. Activity increase is attributed to the formation of localized hot spots in the catalyst bed (Robinson et al. 2020). During the catalytic experiments hot spots were observed from the cavity facing the catalyst bed. As a result, the measured bulk temperatures of the catalyst bed were less than the actual temperature of the active sites of the catalysts. Thus, a temperature of 450 °C became sufficient to achieve 63.5% ethane conversion. However, according to the thermodynamic calculations, it was found that the equilibrium conversion at 400 °C was almost zero. This value increased to nearly 5, 10, 18 and 25% at temperatures of 500, 550, 600 and 600 °C, respectively. It is seen that the experimental

Table 2: Catalytic activity results of 5Cr@KIT-6 catalyst at different temperatures (GHSV: 18,000 ml/h.g_{cat}, Et/Ar: 1/2).

Temperature °C	Ethane conversion%	C_2H_4/H_2	Selectivity				Yield			
			H_2	C_2H_4	CH_4	C_2H_2	H_2	C_2H_4	CH_4	C_2H_2
350	2.1	0.87	1.09	0.95	-	–	0.02	0.02	-	–
400	8.0	1.02	0.98	1.00	-	–	0.08	0.08	-	–
450	63.5	0.91	0.93	0.85	0.19	–	0.59	0.54	0.12	–
500	82.8	0.73	1.03	0.75	0.23	0.017	0.86	0.61	0.19	0.014
550	87.2	0.68	1.05	0.71	0.26	0.017	0.91	0.62	0.23	0.015
600	90.9	0.64	1.06	0.68	0.28	0.014	0.97	0.62	0.25	0.013
650	92.0	0.40	1.26	0.50	0.36	0.016	1.16	0.46	0.33	0.015

conversion values obtained in this study are higher than the equilibrium values due to the higher catalyst active sites temperatures. This is the main advantage of using microwave heated reactor in catalytic reactions.

Kim et al. (2001) studied the ethane dehydrogenation with microwave heating system. They compared their experimental ethane conversions with the equilibrium conversion at different temperatures and concluded that ethane conversions achieved in the microwave-heated reactor system are 10–15% greater than the equilibrium conversions. In another study carried out with a microwave heating system, Zhang et al. (2003) investigated H_2S conversion. They compared conventional heating and microwave heating system results with the equilibrium conversions. They found that H_2S conversion in microwave system was higher than that obtained with conventional system at the same temperature and also higher than the equilibrium H_2S conversions. This is one of the main reasons for using a microwave heating system.

To investigate the effect of feed composition on the catalytic activity 5Cr@KIT-6 catalyst was tested at different feed ratios of Et/Ar: 1/2, 1/1, and 2/1 at 450 °C. Table 3 summarizes the catalytic activity results. As expected, ethane conversion decreases as the feed ratio increases. In the experiments carried out with different feed ratios of Et/Ar, ethylene selectivity and hydrogen selectivity values were found close to each other. Additionally, small amount of CH_4 was detected in the product stream. These results confirmed that undesired side reactions occurred in small amount. It was seen that the highest ethane conversion was obtained with a feed of Et/Ar: 1/2 (63.5%). However, the highest C_2H_4/H_2 ratio was obtained as 0.99 with a feed ratio of Et/Ar: 1/1.

To understand the effect of different metal on the catalytic activity, Co-containing mono-metallic (5Co@KIT-6) and bi-metallic (2.5Cr2.5Co@KIT-6) catalysts were tested at 450 °C and with a feed ratio of Et/Ar: 1/2. Figure 10 shows the time-dependent ethane conversion and selectivity values of the catalysts after 20th minutes of the reaction at which microwave heated reactor system stabilizes. Catalytic activity results obtained with different catalysts are summarized in Table 4. The 5Cr@KIT-6 catalyst was found to exhibit stable catalytic activity among the catalysts tested. In the 5Co@KIT-6 catalyst, it has been observed that ethane conversion decreases by almost half of the initial value as the reaction progresses. The presence of CH_4 in the product relates with the occurrence of side reactions, such as ethane decomposition (R3: $C_2H_6 \rightarrow CH_4 + H_2 + C$, R4: $C_2H_6 \rightarrow CH_4 + 1/2C_2H_4$) and ethylene decomposition (R5: $C_2H_4 \rightarrow CH_4 + C$). It is seen that the highest ratio of C_2H_4 to H_2 (0.98), which is a measure of the small amount of side reactions, was obtained with the 2.5Cr2.5Co@KIT-6 catalyst. When compared to the results of the 5Cr@KIT-6 catalyst, it can be said that the addition of Co to the Cr-containing catalyst increases the C_2H_4/H_2 ratio.

In the study of Ji et al. (2018), it was reported that there is a direct relation between surface acidity and ethane conversions. They prepared Mo/ZSM-5 and phosphorus-modified Mo/ZSM-5 catalysts to understand the effect of surface acidity on aromatization of ethane. They concluded that the catalyst having the highest Lewis acidity exhibited the highest ethane conversion. In this study, there was a small difference between the Lewis acidity of the catalysts. Therefore, no direct relation was found between surface acidity and ethane dehydrogenation activity. Since other surface properties (BET surface area, pore diameter, pore volume, etc.) of the catalysts are similar, it is thought that physicochemical properties may have little effect on catalytic activity in this study. However, the effect of Co addition to the Cr-containing catalyst on C_2H_4/H_2 ratio is quite significant. High ethylene selectivity was achieved with the 2.5Cr2.5Co@KIT-6 catalyst, and thus the C_2H_4/H_2 ratio increased to 0.98. Another important issue to be considered in this study is the use of a microwave heating system. The ethane conversion values reached at each temperature in this work were higher than the theoretical equilibrium conversions. The reason to get high conversion is using the microwave heating system. It is one of the most important results of this study that high hydrogen yield and ethylene

Table 3: Catalytic activity results obtained with different feed ratios (T = 450 °C GHSV: 18,000 ml/h.g_{cat}).

Catalyst	Et/Ar	Ethane conversion %	C_2H_4/H_2	Selectivity			Yield		
				H_2	C_2H_4	CH_4	H_2	C_2H_4	CH_4
5Cr@KIT-6	1/2	63.5	0.91	0.93	0.85	0.19	0.59	0.54	0.12
	1/1	46.7	0.99	0.92	0.91	0.14	0.43	0.42	0.06
	2/1	39.5	0.98	0.91	0.89	0.16	0.36	0.34	0.07

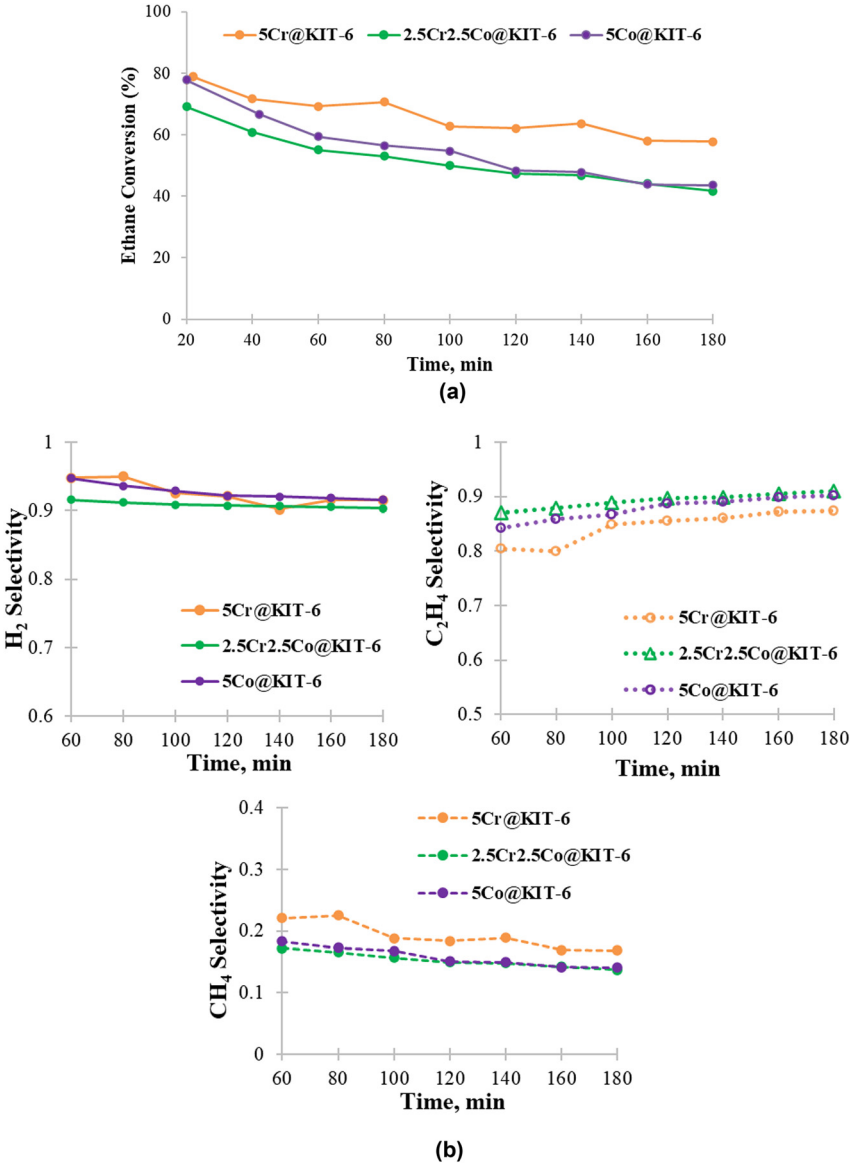

Figure 10: Time-dependent a) ethane conversion and b) product selectivity of the catalysts at 450 °C (Et/Ar: 1/2).

Table 4: Catalytic activity results obtained with different catalysts (T = 450 °C, Et/Ar: 1/2, GHSV: 18,000 ml/h.g_{cat}).

Catalyst	Et/Ar	Ethane conversion %	C_2H_4/H_2	Selectivity			Yield		
				H_2	C_2H_4	CH_4	H_2	C_2H_4	CH_4
5Cr@KIT-6	1/2	63.5	0.91	0.93	0.85	0.19	0.59	0.54	0.12
2.5Cr2.5Co@KIT-6	1/2	48.3	0.98	0.91	0.89	0.15	0.44	0.43	0.07
5Co@KIT-6	1/2	50.6	0.95	0.93	0.88	0.16	0.47	0.44	0.08

production can be realized by dehydrogenation of ethane using microwave heating even at lower temperatures. In the literature, MoFe/ZSM-5 catalyst was tested for ethane dehydrogenation reaction at 375 °C bulk temperature and exhibited 20% ethane conversion and 50% ethylene selectivity in microwave heating reactor system (Robinson et al. 2020). In another study, Kim et al. (2001) obtained 73% ethane conversion with 87% ethylene selectivity using Korean anthracite catalyst at about 700 °C reaction site temperature in microwave heating system.

4 Conclusion

Mesoporous KIT-6 supported Cr and Co-based catalysts were investigated for hydrogen production via microwave-assisted non-oxidative ethane dehydrogenation. KIT-6 support having well-ordered three-dimensional mesoporous structure organized in body-centered cubic array was prepared by hydrothermal method. The N_2 adsorption–desorption isotherms of KIT-6 support and metal-impregnated catalysts were Type IV which is the indication of mesopore structure. Even after high metal loading, the preservation of mesopore structure was confirmed by XRD and N_2 adsorption–desorption analyses. The pyridine adsorbed DRIFT analysis revealed that catalysts have Lewis acid sites. The 5Cr@KIT-6 catalyst exhibited 63.5% ethane conversion with a feed ratio of Et/Ar:1/2 at 450 °C. The effect of ethane feed ratio was examined and as expected, ethane conversion decreases as the feed ratio increases. The addition of Co to the Cr-containing catalyst positively affected the catalytic activity. High ethylene selectivity (C_2H_4/H_2 = 0.98) was obtained with the 2.5Cr2.5Co@KIT-6 catalyst. In the experiments conducted at different temperatures (350–650 °C), the ethane conversion increases with the increasing temperature due to the endothermic nature of the ethane decomposition reaction. The experimental conversion values observed higher than the equilibrium conversions were attributed to the high temperatures of the catalyst active sites. At high reaction temperatures (above 450 °C), side reactions began to occur and while hydrogen selectivity increased, ethylene selectivity decreased. The increase in the H_2 yield and the formation of CH_4 and C_2H_2 in the product stream could be attributed to the occurrence of endothermic ethane decomposition and ethylene decomposition side reactions. The ethane conversion values at different temperatures were found to be higher than the thermodynamic equilibrium conversions. It was concluded that microwave heating reduces the bulk catalyst temperatures and provides activity increase due to the formation of localized hot spots in the catalyst bed. This result is an indication of energy saving advantage of microwave heating system, which is very important especially for endothermic catalytic reactions.

Acknowledgments: The author thanks to the Central Laboratory of METU for the characterization results of the synthesized materials.
Author contributions: All the authors have accepted responsibility for the entire content of this submitted manuscript and approved submission.
Research funding: This work was financially supported by Gazi University Research Fund (Grant No. 06/2019-02).
Conflict of interest statement: The authors declare no conflicts of interest regarding this article.

References

Ahn, S. J., G. N. Yun, A. Takagaki, R. Kikuchi, and S. T. Oyama. 2018. "Effects of Pressure, Contact Time, Permeance, and Selectivity in Membrane Reactors: The Case of the Dehydrogenation of Ethane." *Separation and Purification Technology* 194: 197–206.

Alalwan, H. A., D. M. Cwiertny, and V. H. Grassian. 2017. "Co_3O_4 Nanoparticles as Oxygen Carriers for Chemical Looping Combustion: A Materials Characterization Approach to Understanding Oxygen Carrier Performance." *Chemical Engineering Journal* 319: 279–87.

Anandhi, J. T., S. L. Rayer, and T. Chithambarathanu. 2017. "Synthesis, FTIR Studies and Optical Properties of Aluminium Doped Chromium Oxide Nanoparticles by Microwave Irradiation at Different Concentrations." *Chemical and Materials Engineering* 5 (2): 43.

Arbag, H. 2018. "Effect of Impregnation Sequence of Mg on Performance of Mesoporous Alumina Supported Ni Catalyst in Dry Reforming of Methane." *International Journal of Hydrogen Energy* 43 (13): 6561–74.

Ausavasukhi, A., and T. Sooknoi. 2014. "Tunable Activity of [Ga] HZSM-5 with H_2 Treatment: Ethane Dehydrogenation." *Catalysis Communications* 45: 63–8.

Ayad, M. M., N. A. Salahuddin, A. A. El-nasr, and N. L. Torad. 2016. "Microporous and Mesoporous Materials Amine-functionalized Mesoporous Silica KIT-6 as a Controlled Release Drug Delivery Carrier." *Microporous and Mesoporous Materials* 229: 166–77.

Bai, X., S. Tiwari, B. Robinson, C. Killmer, L. Li, and J. Hu. 2018. "Microwave Catalytic Synthesis of Ammonia from Methane and Nitrogen." *Catalysis Science and Technology* 8 (24): 6302–5.

Bugrova, T. A., V. V. Dutov, V. A. Svetlichnyi, V. Cortés Corberán, and G. V. Mamontov. 2019. "Oxidative Dehydrogenation of Ethane with CO_2 over CrO_x Catalysts Supported on Al_2O_3, ZrO_2, CeO_2 and $Ce_xZr_{1-x}O_2$." *Catalysis Today* 333: 71–80.

Chen, S., X. Pan, C. Miao, H. Xie, G. Zhou, Z. Jiao, and X. Zhang. 2018. "Study of Catalytic Hydrodeoxygenation Performance for the Ni/KIT-6 Catalysts." *Journal of Saudi Chemical Society* 22 (5): 614–27.

Chirra, S., S. Siliveri, A. Kumar, A. Srinath, G. Sripal, and R. Gujjula. 2019. "Pd – KIT – 6: Synthesis of a Novel Three – Dimensional Mesoporous Catalyst and Studies on its Enhanced Catalytic Applications." *Journal of Porous Materials* 26: 1667–77.

Cychosz, K. A., and M. Thommes. 2018. "Progress in the Physisorption Characterization of Nanoporous Gas Storage Materials." *Engineering* 4 (4): 559–66.

Dangwal, S., R. Liu, and S. J. Kim. 2017. "High-temperature Ethane Dehydrogenation in Microporous Zeolite Membrane Reactor: Effect of Operating Conditions." *Chemical Engineering Journal* 328: 862–72.

Dragoi, B., A. Ungureanu, A. Chirieac, V. Hulea, S. Royer, and E. Dumitriu. 2013. "Enhancing the Performance of SBA-15-Supported Copper Catalysts by Chromium Addition for the

Chemoselective Hydrogenation of Trans-cinnamaldehyde." *Catalysis Science and Technology* 3 (9): 2319–29.

Eslek Koyuncu, D. D. 2020. "Microwave-assisted Non-oxidative Ethane Dehydrogenation over Different Carbon Materials." *Diamond and Related Materials*. in press.

Fernandes, F. R. D., F. G. H. S. Pinto, E. L. F. Lima, L. D. Souza, V. P. S. Caldeira, and A. G. D. Santos. 2018. "Influence of Synthesis Parameters in Obtaining KIT-6 Mesoporous Material." *Applied Sciences* 8 (5), https://doi.org/10.3390/app8050725.

Gopinatha, S., and N. Nagarajanb. 2015. "Energy Based Reliable Multicast Routing Protocol for Packet Forwarding in MANET." *Journal of Applied Research and Technology* 13: 374–81.

Heracleous, E., and A. A. Lemonidou. 2006. "Reaction Pathways of Ethane Oxidative and Non-oxidative Dehydrogenation on Î³-Al_2O_3 Studied by Temperature-programmed Reaction (TP-reaction)." *Catalysis Today* 112 (1–4): 23–7.

Huang, Y., X. Dong, Y. Yu, and M. Zhang. 2017. "Kinetic Monte Carlo Study of Vinyl Acetate Synthesis from Ethylene Acetoxylation on Pd(100) and Pd/Au(100)." *Applied Surface Science* 423: 793–9.

Jan, O., and F. L. P. Resende. 2018. "Liquid Hydrocarbon Production via Ethylene Oligomerization over Ni-Hî." *Fuel Processing Technology* 179: 269–76.

Ji, Z., H. Lv, X. Pan, and X. Bao. 2018. "Enhanced Ethylene Selectivity and Stability of Mo/ZSM5 upon Modification with Phosphorus in Ethane Dehydrogenation." *Journal of Catalysis* 361: 94–104.

Jira, R. 2009. "Acetaldehyde from Ethylene – A Retrospective on the Discovery of the Wacker Process." *Angewandte Chemie – International Edition* 48 (48): 9034–7.

Karthikeyan, G. G., G. Boopathi, A. Pandurangan, G. Boopathi, and A. Pandurangan. 2018. "Facile Synthesis of Mesoporous Carbon Spheres Using 3D Cubic Fe-KIT-6 by CVD Technique for the Application of Active Electrode Materials in Supercapacitors." *ACS Omega* 3: 16658–71.

Ke, C., Y. Zhang, Y. Gao, Y. Pan, B. Li, Y. Wang, and R. Ruan. 2019. "Syngas Production from Microwave-assisted Air Gasification of Biomass: Part 1 Model Development." *Renewable Energy* 140: 772–8.

Kim, D. K., C. Y. Cha, W. T. Lee, and J. H. Kim. 2001. "Microwave Dehydrogenation of Ethane to Ethylene." *Journal of Industrial and Engineering Chemistry* 7 (6): 363–74.

Kishor, R., and A. K. Ghoshal. 2017. "Understanding the Hydrothermal, Thermal, Mechanical and Hydrolytic Stability of Mesoporous KIT-6: A Comprehensive Study." *Microporous and Mesoporous Materials* 242: 127–35.

Kleitz, F., S. H. Choi, and R. Ryoo. 2003. "Cubic Ia3d Large Mesoporous Silica: Synthesis and Replication to Platinum Nanowires, Carbon Nanorods and Carbon Nanotubes." *Chemical Communications* 9 (17): 2136–7.

Leth, K. T., A. K. Rovik, M. S. Holm, M. Brorson, H. J. Jakobsen, J. Skibsted, and C. H. Christensen. 2008. "Synthesis and Characterization of Conventional and Mesoporous Ga-MFI for Ethane Dehydrogenation." *Applied Catalysis A: General* 348 (2): 257–65.

Li, B., X. Luo, J. Huang, X. Wang, and Z. Liang. 2017. "One – Pot Synthesis of Ordered Mesoporous Cu – KIT – 6 and its Improved Catalytic Behavior for the Epoxidation of Styrene : Effects of the pH Value of the Initial Gel." *Chinese Journal of Catalysis* 38 (3): 518–28.

Liu, H., S. Xu, G. Zhou, G. Huang, S. Huang, and K. Xiong. 2018a. CO_2 Hydrogenation to Methane over Co/KIT-6 Catalyst : Effect of Reduction Temperature.351 65-73.

Liu, J., P. He, L. Wang, H. Liu, Y. Cao, and H. Li. 2018b. "An Efficient and Stable Cu/SiO_2 Catalyst for the Syntheses of Ethylene Glycol and Methanol via Chemoselective Hydrogenation of Ethylene Carbonate." *Chinese Journal of Catalysis* 39 (8): 1283–93.

Lu, X., H. Xu, J. Yan, W. J. Zhou, A. Liebens, and P. Wu. 2018. "One-pot Synthesis of Ethylene Glycol by Oxidative Hydration of Ethylene with Hydrogen Peroxide over Titanosilicate Catalysts." *Journal of Catalysis* 358: 89–99.

Megia, P. J., A. Carrero, J. A. Calles, and A. J. Vizcaino. 2019. "Hydrogen Production from Steam Reforming of Acetic Acid as a Model Compound of the Aqueous Fraction of Microalgae HTL Using Co-M/SBA-15 (M: Cu, Ag, Ce, Cr) Catalysts." *Catalysts* 9: 1013–31.

Merkache, R., I. Fechete, M. Maamache, M. Bernard, P. Turek, K. Al-Dalama, and F. Garin. 2015. "3D Ordered Mesoporous Fe-KIT-6 Catalysts for Methylcyclopentane (MCP) Conversion and Carbon Dioxide (CO_2) Hydrogenation for Energy and Environmental Applications." *Applied Catalysis A: General* 504: 672–81.

Moslemi, A., A. Najafi Chermahini, J. Najafi Sarpiri, S. Rezaei, and M. Barati. 2019. "$VOHPO_4.5H_2O$/KIT-6 Composites: Preparation and Their Application in Extractive and Catalytic Oxidation Desulfurization of Benzothiophene and Dibenzothiphene." *Journal of the Taiwan Institute of Chemical Engineers* 97: 237–46.

Ng, S., C. Fairbridge, S. Mutyala, Y. Liu, M. R. Bélanger, and J. R. J. Paré. 2013. "Microwave-assisted Conversion of Ethane to Ethylene." *Applied Petrochemical Research* 3 (1–2): 55–61.

Qiu, C., Q. Meng, M. Panchal, C. Li, and B. Wu. 2020. "Enhanced Fischer-Tropsch Activity in Ammonium Nitrate Pretreated Cobalt-Silica Catalyst." *Catalysis Communications* 147: 106149.

Quijada, R., R. Rojas, G. Bazan, Z. J. A. Komon, R. S. Mauler, and G. B. Galland. 2001. "Synthesis of Branched Polyethylene from Ethylene by Tandem Action of Iron and Zirconium Single Site Catalysts." *Macromolecules* 34 (8): 2411–17.

Rahmani, F., M. Haghighi, and M. Amini. 2015. "The Beneficial Utilization of Natural Zeolite in Preparation of Cr/clinoptilolite Nanocatalyst Used in CO_2-oxidative Dehydrogenation of Ethane to Ethylene." *Journal of Industrial and Engineering Chemistry* 31: 142–55.

Rahmanzadeh, L., and M. Taghizadeh. 2019. "Hydrogen Production from Ethanol Steam Reforming Using Ce- and La-modified Mesoporous MCM-41 Supported Nickel-based Catalysts." *International Journal of Chemical Reactor Engineering* 17 (8): 1–17.

Robinson, B., A. Caiola, X. Bai, V. Abdelsayed, D. Shekhawat, and J. Hu . 2020. "Catalytic Direct Conversion of Ethane to Value-Added Chemicals under Microwave Irradiation." *Catalysis Today*: 0–1, https://doi.org/10.1016/j.cattod.2020.03.001.

Ruelas-Leyva, J. P., A. Mata-Martinez, A. Talavera-LÃ³pez, S. A. GÃ³mez, S. A. Jimenez-Lam, and G. A. Fuentes. 2018. "Dehydrogenation of Propane to Propylene with Highly Stable Catalysts of Pt-Sn Supported over Mesoporous Silica KIT-6." *International Journal of Chemical Reactor Engineering* 16 (10): 1–10.

Saito, H., and Y. Sekine. 2020. "Catalytic Conversion of Ethane to Valuable Products through Non-oxidative Dehydrogenation and Dehydroaromatization." *RSC Advances* 10 (36): 21427–53.

Shen, W., Y. Wang, X. Shi, N. Shah, F. Huggins, S. Bollineni, M. Seehra, and G. Huffman. 2007. "Catalytic Nonoxidative Dehydrogenation

of Ethane over Fe-Ni and Ni Catalysts Supported on Mg(Al)O to Produce Hydrogen and Easily Purified Carbon Nanotubes." *Energy and Fuels* 21 (6): 3520–9.

Smith, D. K., and L. G. Berry. 1974. *Selected Powder Diffraction Data for Minerals*, 1st ed. Pennsylvania: Joint Committee on Powder Diffraction Standards.

Son, W. J., J. S. Choi, and W. S. Ahn. 2008. "Adsorptive Removal of Carbon Dioxide Using Polyethyleneimine-loaded Mesoporous Silica Materials." *Microporous and Mesoporous Materials* 113 (1–3): 31–40.

Sun, J., W. Wang, and Q. Yue. 2016. "Review on Microwave-Matter Interaction Fundamentals and Efficient Microwave-associated Heating Strategies." *Materials* 9 (4), https://doi.org/10.3390/ma9040231.

Sun, P., G. Siddiqi, W. C. Vining, M. Chi, and A. T. Bell. 2011. "Novel Pt/Mg(In)(Al)O Catalysts for Ethane and Propane Dehydrogenation." *Journal of Catalysis* 282 (1): 165–74.

Taghizadeh, M., H. Akhoundzadeh, and A. Rezayan. 2018. "ScienceDirect Excellent Catalytic Performance of 3D-Mesoporous KIT-6 Supported Cu and Ce Nanoparticles in Methanol Steam Reforming." *International Journal of Hydrogen Energy* 43 (24): 10926–37.

Taifan, W. E., G. X. Yan, and J. Baltrusaitis. 2017. "Surface Chemistry of MgO/SiO_2 Catalyst during the Ethanol Catalytic Conversion to 1,3-butadiene: In-Situ DRIFTS and DFT Study." *Catalysis Science and Technology* 7 (20): 4648–68.

Tan, Y., S. Wang, L. Li, B. Meng, J. Chen, Z. Yang, K. Yan, and X. Qin. 2019. "Application of Microwave Heating for Methane Dry Reforming Catalyzed by Activated Carbon." *Chemical Engineering and Processing – Process Intensification* 145: 107662.

Thommes, M., K. Kaneko, A. V. Neimark, J. P. Olivier, F. Rodriguez-Reinoso, J. Rouquerol, and K. S. W. Sing. 2015. "Physisorption of Gases, with Special Reference to the Evaluation of Surface Area and Pore Size Distribution (IUPAC Technical Report)." *Pure and Applied Chemistry* 87 (9–10): 1051–69.

Tsyganok, A., R. G. Green, J. B. Giorgi, and A. Sayari. 2007. "Non-oxidative Dehydrogenation of Ethane to Ethylene over Chromium Catalysts Prepared from Layered Double Hydroxide Precursors." *Catalysis Communications* 8 (12): 2186–93.

Varisli, D., C. Korkusuz, and T. Dogu. 2017. "Microwave-assisted Ammonia Decomposition Reaction over Iron Incorporated Mesoporous Carbon Catalysts." *Applied Catalysis B: Environmental* 201: 370–80.

Vincent, I., and D. Bessarabov. 2018. "Low Cost Hydrogen Production by Anion Exchange Membrane Electrolysis: A Review." *Renewable and Sustainable Energy Reviews* 81: 1690–704.

Wang, L. C., Y. Zhang, J. Xu, W. Diao, S. Karakalos, B. Liu, X. Song, W. Wu, T. He, and D. Ding. 2019. "Non-oxidative Dehydrogenation of Ethane to Ethylene over ZSM-5 Zeolite Supported Iron Catalysts." *Applied Catalysis B: Environmental* 256: 117816.

Wang, W., R. Qi, W. Shan, X. Wang, Q. Jia, J. Zhao, C. Zhang, and H. Ru. 2014. "Microporous and Mesoporous Materials Synthesis of KIT-6 Type Mesoporous Silicas with Tunable Pore Sizes, Wall Thickness and Particle Sizes via the Partitioned Cooperative Self-Assembly Process." *Microporous and Mesoporous Materials* 194: 167–73,.

Wegener, E. C., Z. Wu, H. T. Tseng, J. R. Gallagher, Y. Ren, R. E. Diaz, F. H. Ribeiro, and J. T. Miller. 2018. "Structure and Reactivity of Pt–In Intermetallic Alloy Nanoparticles: Highly Selective Catalysts for Ethane Dehydrogenation." *Catalysis Today* 299: 146–53.

Wildfire, C., V. Abdelsayed, D. Shekhawat, and M. J. Spencer. 2018. "Ambient Pressure Synthesis of Ammonia Using a Microwave Reactor." *Catalysis Communications* 115: 64–7.

Wu, J., Z. Peng, and A. T. Bell. 2014. ""Effects of Composition and Metal Particle Size on Ethane Dehydrogenation over Pt_xSn_{100-x}/Mg(Al)O (70–100)." *Journal of Catalysis* 311: 161–8.

Xia, D., Y. Chen, C. Li, C. Liu, and G. Zhou. 2018. "Carbon Dioxide Reforming of Methane to Syngas over Ordered Mesoporous Ni/KIT-6 Catalysts." *International Journal of Hydrogen Energy* 43 (45): 20488–99.

Xiang, Y., H. Wang, J. Cheng, and J. Matsubu. 2018. "Progress and Prospects in Catalytic Ethane Aromatization." *Catalysis Science and Technology* 8 (6): 1500–16.

Xu, J., Y. Hong, M. J. Cheng, B. Xue, and Y. X. Li. 2019. "Vanadyl Acetylacetonate Grafted on Ordered Mesoporous Silica KIT-6 and its Enhanced Catalytic Performance for Direct Hydroxylation of Benzene to Phenol." *Microporous and Mesoporous Materials* 285: 223–30.

Xu, L., C. Wang, and J. Guan. 2014. "Preparation of Acid-Base Bifunctional Mesoporous KIT-6 (KIT: Korea Advanced Institute of Science and Technology) and its Catalytic Performance in Knoevenagel Reaction." *Journal of Solid State Chemistry* 213: 250–5.

Xu, W., J. Zhou, Z. Su, Y. Ou, and Z. You. 2016. "Microwave Catalytic Effect: A New Exact Reason for Microwave-Driven Heterogeneous Gas-phase Catalytic Reactions." *Catalysis Science and Technology* 6 (3): 698–702.

Zhang, X., D. O. Hayward, and D. M. P. Mingos. 2003. "Effects of Microwave Dielectric Heating on Heterogeneous Catalysis." *Catalysis Letters* 88: 33–8.

Zhang, C., H. Yue, Z. Huang, S. Li, G. Wu, X. Ma, and J. Gong. 2013. "Hydrogen Production via Steam Reforming of Ethanol on Phyllosilicate- Derived Ni/SiO_2: Enhanced Metal-Support Interaction and Catalytic Stability." *ACS Sustainable Chemistry and Engineering* 1 (1): 161–73.

Zhao, X. Q., S. Veintemillas-Verdaguer, O. Bomati-Miguel, M. P. Morales, and H. B. Xu. 2005. "Thermal History Dependence of the Crystal Structure of Co Fine Particles." *Physical Review B – Condensed Matter and Materials Physics* 71 (2), https://doi.org/10.1103/PhysRevB.71.024106.